J Mater Sci: Mater Electron (2015) 26:3970–3975
DOI 10.1007/s10854-015-2932-4

Influence of lithium disilicate addition on the dielectric properties of chemically synthesized $CaCu_3Ti_4O_{12}$

T. C. Porfirio[1] · E. N. S. Muccillo[1]

Received: 8 December 2014 / Accepted: 10 March 2015 / Published online: 14 March 2015

Abstract The effects of the method of synthesis along with the introduction of a sintering aid on the electric and dielectric properties of $CaCu_3Ti_4O_{12}$ were investigated in detail. The mixed oxide with perovskite structure was synthesized by the coprecipitation method. Polycrystalline specimens were prepared by adding 0.5 mol% $Li_2Si_2O_5$ to the mixed oxide followed by sintering in the 1000–1100 °C range for 12 h. A high density value was obtained for sintering at a temperature as low as 1000 °C. Average grain sizes of sintered specimens are of the same order of magnitude as those of specimens prepared by the same method without the additive. The activation energy values for electric conduction were found to be 0.1 eV (grain) and varying from 0.4 to 0.6 eV (grain boundary). The dielectric properties are similar to those of specimens without the additive. The overall results evidence the possibility of reduction of the sintering temperature by about 100 °C with the introduction of a small amount of lithium disilicate while keeping the dielectric properties of pure $CaCu_3Ti_4O_{12}$.

1 Introduction

The perovskite $CaCu_3Ti_4O_{12}$, CCTO, with a body centered cubic structure (space group *Im-3*) has attracted much attention in recent years, due to the combination of its dielectric properties, specifically the giant dielectric permittivity ($\varepsilon' > 1000$) and the small dielectric loss ($\tan \delta < 1$), and because of its thermal stability in wide temperature and frequency ranges [1, 2]. This polycrystalline ceramic constitutes a promising material for applications in microelectronics such as microwave, supercapacitors and memory devices [3, 4].

Several reports may be found on the origin of the special properties of CCTO, supporting the model based on extrinsic factors to explain the main dielectric features of polycrystalline CCTO [5–10]. This ceramic material consists of semiconductor grains along with insulating grain boundaries. Moreover, defects such as stoichiometry deviation, different oxidation states of copper and titanium, and segregation of copper at grain boundaries, contribute to the heterogeneity of the perovskite material. Because of such complex microstructure, a model based on internal barrier layer capacitance (IBLC) has been widely accepted to explain the mechanism responsible for the dielectric behavior of polycrystalline CCTO [5].

Most of previous studies were conducted in polycrystalline ceramics prepared by the conventional solid state reaction method [1, 3–13]. Few works have employed a solution method to obtain a more homogeneous microstructure [14–16]. In addition, the dielectric properties of CCTO are known to depend on the processing conditions [17]. In this context, there are few studies on the effects produced by the introduction of sintering aids. Recent reports on sintering aids are related to the addition of caulinite [18], or borosilicate glass-type additives such as $BaO–B_2O_3–SiO_2$ [19] and $SrO–B_2O_3–SiO_2$ [20]. These additives were found to improve the dielectric properties of CCTO.

Here is reported for the first time the effects of the method of synthesis along with the use of a non-borosilicate glass-type additive on the dielectric and electric properties of CCTO. The main purpose is to verify the

✉ E. N. S. Muccillo
enavarro@usp.br

[1] Energy and Nuclear Research Institute – IPEN, PO Box 11049, São Paulo, SP 05422-970, Brazil

effect of both the method of synthesis and of a densifying additive on the improvement of the microstructure of CCTO, thereby contributing to the understanding of the influence of extrinsic factors on the microstructure-property relationship of this polycrystalline mixed oxide.

2 Experimental

$CaCu_3Ti_4O_{12}$ was synthesized by the coprecipitation method with reagent grade calcium and copper nitrates, and titanium isopropoxide, as starting materials. The overall coprecipitation process is similar to that described elsewhere [21]. Stoichiometric proportions of the starting aqueous nitrate solutions (1 mol L^{-1}) were mixed together and homogenized. The titanium isopropoxide was added dropwise to an alcoholic solution of nitric acid to obtain the titanium nitrate solution. These solutions were thoroughly mixed under constant stirring. The cation solution was added to an alcoholic solution of oxalic acid (0.05 mol L^{-1}, pH = 3) promoting the coprecipitation of the desired cations. The concentration of each solution was verified by gravimetry. After precipitation completion, the as-prepared material was washed with absolute ethyl alcohol and isopropyl alcohol. The coprecipitated material was subsequently dispersed in *n*-butyl alcohol followed by azeotropic distillation for water removal. Afterwards, the as-prepared material was dried in an oven, deagglomerated in an agate mortar and calcined at 700 and 800 °C for 1, 4 and 8 h. After calcination, the CCTO powder was divided into two fractions. To one fraction, 2 wt% polyvinyl alcohol, PVA, was added. This binder material is usually introduced to increase the mechanical strength of the green compacts. The other fraction was mixed to 0.5 mol% lithium disilicate, $Li_2Si_2O_5$ (LSO) as a sintering aid. In the latter, no binder was added. The content of lithium disilicate was chosen after preliminary experiments, when its content was varied up to 1.5 mol%.

$Li_2Si_2O_5$ was prepared by solid state reaction between lithium carbonate (P.A.) and amorphous silica (99.9 %). Stoichiometric amounts of the reagents were ball milled for 2 h in alcoholic medium and dried at 50 °C for 24 h. The mixture was then calcined twice at 970 °C for 4 h to obtain the desired composition.

Disc shaped specimens were prepared by uniaxial pressing in a stainless steel die with 55 MPa of applied pressure. Sintering of the green compacts was carried out for 12 h in air in the 1000–1100 °C range.

The temperatures of thermal decomposition and crystallization of the synthesized CCTO were evaluated by simultaneous thermogravimetry, TG, and differential thermal analyses, DTA (Netzsch, STA 409) under synthetic air, heating at a rate of 10 °C min^{-1} from room temperature up to 900 °C. Alpha-alumina was used as standard material in DTA runs. Identification of crystalline phases was carried out by X-ray diffraction (Bruker-AXS, D8 Advance) in the $20° \leq 2\theta \leq 80°$ range with 0.05° step size and 3 s counting time with Cu K_α radiation ($\lambda = 1.5405$ Å). The apparent density of sintered specimens was determined by the water immersion technique, and relative density values were calculated using the theoretical density of 4.90 g cm^{-3} [22]. The morphology of sintered specimens was observed on polished and thermally etched surfaces by field emission gun scanning electron microscopy, FEG-SEM (FEI, Inspect F50). The electric and the dielectric properties of sintered specimens were determined by impedance spectroscopy (Hewlett Packard, 4192A) in the 5 Hz–13 MHz frequency range from room temperature up to 180 °C. These measurements were performed with 100 mV of applied *ac* signal. For these measurements, the parallel surfaces of the disc shaped specimens were metalized by application of silver paste followed by cure at 400 °C.

3 Results and discussion

Figure 1 shows TG and DTA curves of the as-prepared material. The main endothermic events are found at 110 and ~200 °C and are accompanied by weight loss. These events are related to the elimination of physisorbed water (110 °C) and residual *n*-butyl alcohol (200 °C) adsorbed on the surface of the powder particles. The thermal decomposition of the mixed oxalate by elimination of CO and CO_2 with a considerable weight loss is revealed in the DTA curve by the exothermic peak at 306 °C.

Negligible weight loss is observed for temperatures higher than 400 °C. The total weight loss amounts 58 %. The exothermic peak at 430 °C is due to the crystallization

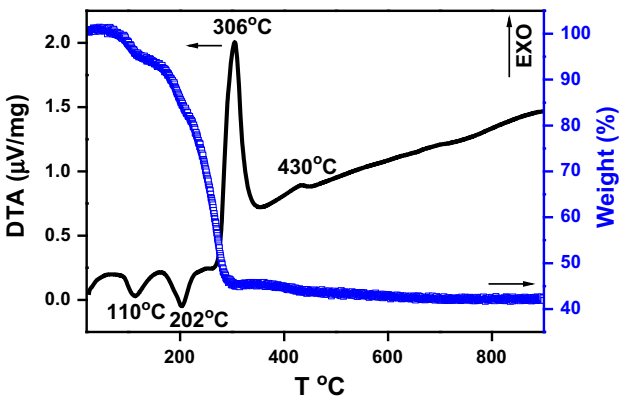

Fig. 1 TG and DTA curves of the coprecipitated CCTO ceramic powder

of the mixed oxide, as corroborated by X-ray diffraction analysis.

Figure 2 shows X-ray diffraction patterns obtained for powders heated up to 430 and 900 °C and cooled down to room temperature, without holding time.

The X-ray diffraction pattern of the prepared material heated up to 430 °C shows reflections characteristic of the precursors of CCTO. After heating up to 900 °C the reflections are typical of $CaCu_3Ti_4O_{12}$ (ICDD 75-1149). In this case, a low intensity diffraction peak (indicated by +) evidences the CuO phase. This reflection is probably related to a partial decomposition of the CCTO phase. This decomposition reaction may result from the expected high reactivity of the synthesized powder.

The calcination temperature was determined by XRD analysis. Figure 3 shows the X-ray diffraction patterns of the dried coprecipitated material calcined at 700 and 800 °C for 1, 4 and 8 h.

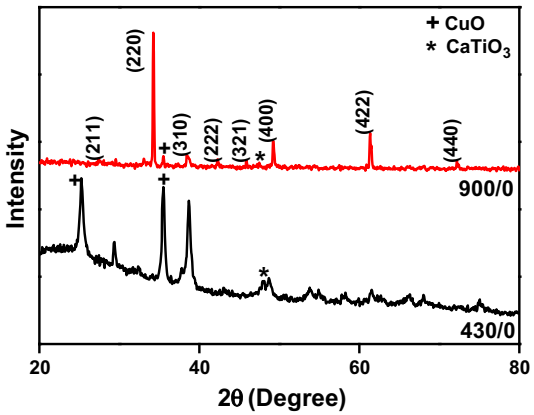

Fig. 2 XRD pattern of the as-prepared material heated up to 430 and 900 °C without holding time, denoted as 430/0 and 900/0, respectively

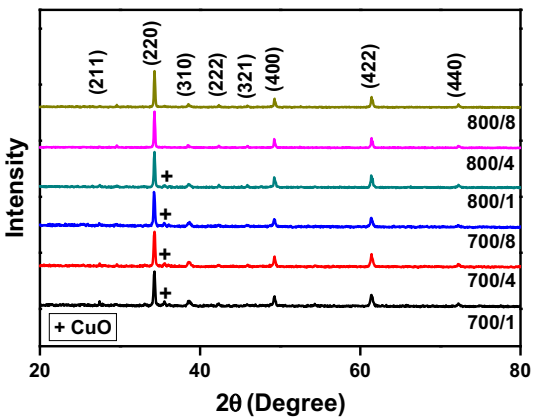

Fig. 3 XRD patterns of the as-prepared material calcined at 700 and 800 °C for 1, 4 and 8 h, denoted as "X/Y", where X and Y are the temperature and holding time, respectively

The diffraction patterns exhibit high intensity and narrow reflections typical of the cubic body centered perovskite structure. It can be noted that after calcination at 700 °C a small diffraction peak due to unreacted CuO is detected, although its intensity gradually decreases with increasing holding time. After calcination at 800 °C for 1 h, the CuO reflection is still present. The powders calcined for 4 and 8 h at 800 °C do not display any extra reflection except those of CCTO, revealing that the formation of the desired phase was completed. Thus, the selected calcination profile was 800 °C for 4 h.

Table 1 Values of relative density (in % of the theoretical value) of sintered CCTO without and with LSO sintered at several temperatures

Sintering profile (°C/h)	Relative density (%)	
	CCTO	CCTO + $Li_2Si_2O_5$
1000/12	–	92.6
1025/12	–	88.2
1050/12	–	92.6
1070/12	90.6	86.1
1080/12	94.3	82.8
1090/12	94.9	80.6
1100/12	95.1	–

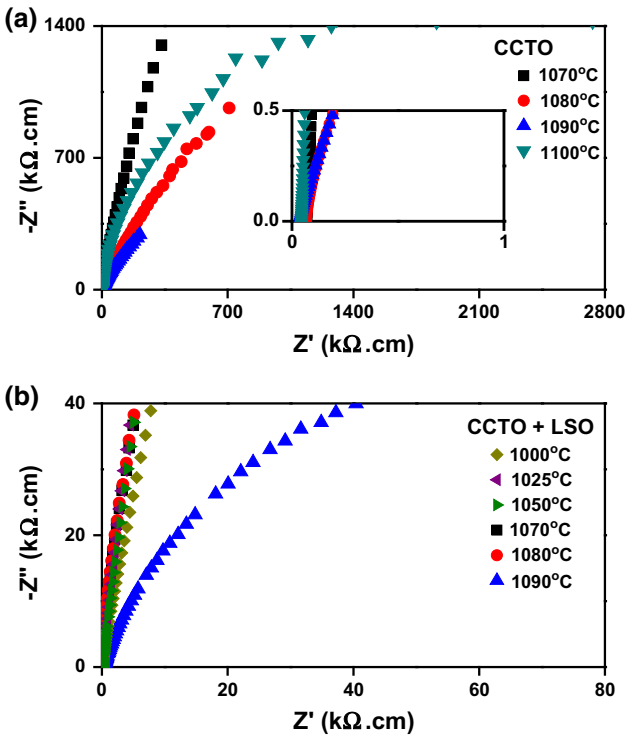

Fig. 4 Impedance diagrams of specimens sintered **a** without and **b** with LSO. In (**a**) the *inset* highlights the high frequency region

Table 1 lists relative density values of specimens with and without the additive sintered at several temperatures for 12 h.

The densification increases with the sintering temperature up to 1090 °C for specimens without the additive reaching 95 % of relative density at 1100 °C. In contrast, the density of specimens containing LSO is approximately 93 % of the theoretical value after sintering at only 1000 °C. This effect may be related to a liquid phase that may have been formed near 1020 °C, the melting temperature of the additive, and the consequent increase in the mass transport, thereby promoting densification at relatively low temperatures.

The $-Z''$ (ω) × Z' (ω) plots measured at room temperature of all sintered specimens are shown in Fig. 4.

The impedance plots consist of a large arc, due to high resistive grain boundaries, with non zero intercept at high frequencies (see inset in Fig. 4a) characteristic of high conducting grains. The bulk or grain conductivity was calculated from the high frequency intercept, and the grain boundary conductivity was determined from the diameter of the low frequency arc. The analysis of the impedance diagrams at all measured temperatures allowed for obtaining the electrical conductivity of the investigated specimens.

The Arrhenius plots of the electrical conductivity of grains and grain boundaries are shown in Figs. 5 and 6 for specimens without and with LSO, respectively. The grain conductivity of specimens without LSO (Fig. 5a) increases with increasing the sintering temperature up to 1090 °C and decreases slightly at 1100 °C. The increase of the grain conductivity for increasing sintering temperature is probably related to the consequent increase in densification of the specimens (Table 1). The opposite trend, observed for specimens sintered at 1100 °C may be associated to changes in the valence of copper, known to occur at such high temperature.

The grain boundary conductivity (Fig. 5b), in contrast, decreases with increasing sintering temperature. This unexpected result shows that with increasing the sintering temperature the grain boundary turns gradually more resistive. This effect, along with the behavior of the grain conductivity, suggests that the change of copper valence

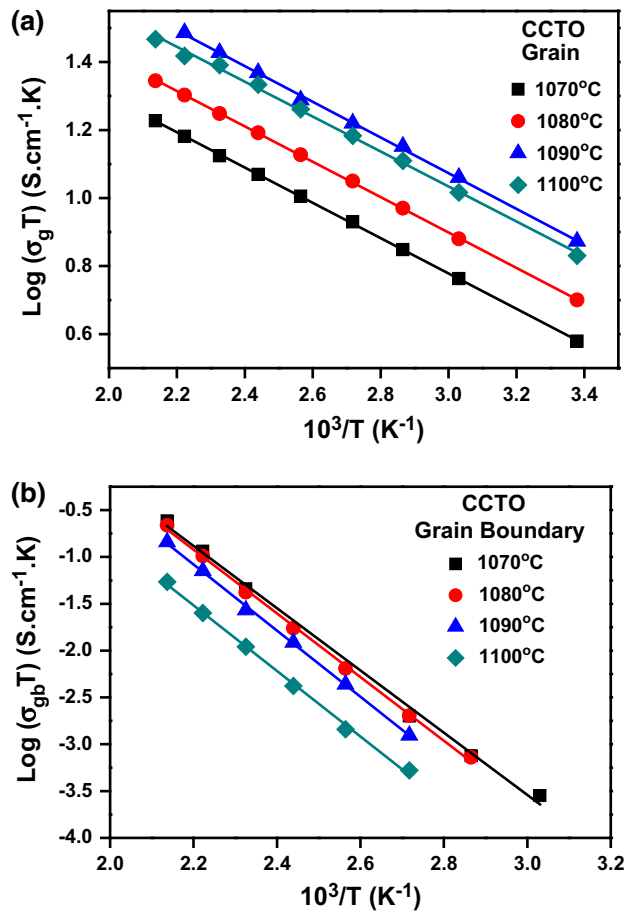

Fig. 5 Arrhenius plots of the electrical conductivity of **a** grains and **b** grain boundaries for specimens without LSO addition

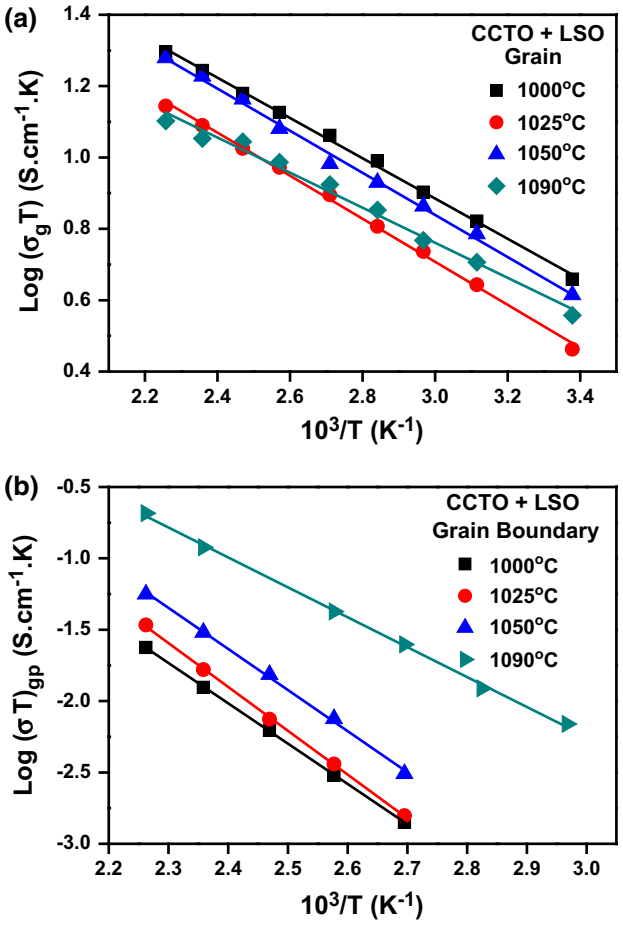

Fig. 6 Arrhenius plots of the electrical conductivity of **a** grains and **b** grain boundaries for specimens with LSO addition

induces cation segregation at the grain boundaries, acting as an additional blocker to the charge carriers. In effect, it has been already proposed that CuO reduces to Cu_2O for temperatures higher than 1000 °C, and during cooling to room temperature its re-oxidation occurs giving rise to a secondary phase at the grain boundaries [12]. Our results indicate that the change of valence is more severe at the interfaces.

The grain conductivity of specimens containing LSO (Fig. 6a) is lower for specimens sintered at 1025 °C, near the melting temperature of the glass additive, and 1090 °C, the highest sintering temperature.

The grain boundary conductivity values of specimens with LSO for 1000, 1025, 1050 and 1090 °C sintering temperatures are shown in Fig. 6b. It can be seen that the grain boundaries become less resistive for increasing sintering temperature. This effect may be attributed to the formation of a more conducting phase at the interfaces.

The activation energy for the grain conductivity is found similar for all specimens ($\sim$0.1 eV). The activation energy for grain boundary conductivity is $\sim$0.65 eV for specimens without additive, in agreement with previous reports [23–25], and varies in the 0.4–0.6 eV range for LSO containing CCTO. In this case, the lower value of the grain boundary activation energy is found for the specimen sintered at 1090 °C, and exhibiting the highest conductivity.

Figure 7 shows FEG-SEM micrographs of CCTO without additive, sintered at 1090 °C and for the specimen containing LSO, sintered at 1000 °C.

The microstructure features in these micrographs are the relatively large grain size, grain pullout and residual porosity. CCTO without additive has polyhedral grains, whereas some curved interfaces may be noted in the specimens with LSO, due to the liquid phase formed during sintering. Table 2 lists values of average grain size, G, determined by the intercept method for the investigated specimens.

The average grain size is found to increase with increasing sintering temperature for specimens without LSO. The capacitance of the grain boundaries normalized by sample geometry is in the nanoFarad range, as expected. The same observation holds for CCTO containing LSO. In this case, the average grain size after sintering at 1000 °C is similar to that of specimens with the additive, sintered at 1090 °C.

Table 2 shows also values of dielectric permittivity and dielectric loss of all studied specimens at 1 kHz at room temperature. The dielectric permittivity is higher for

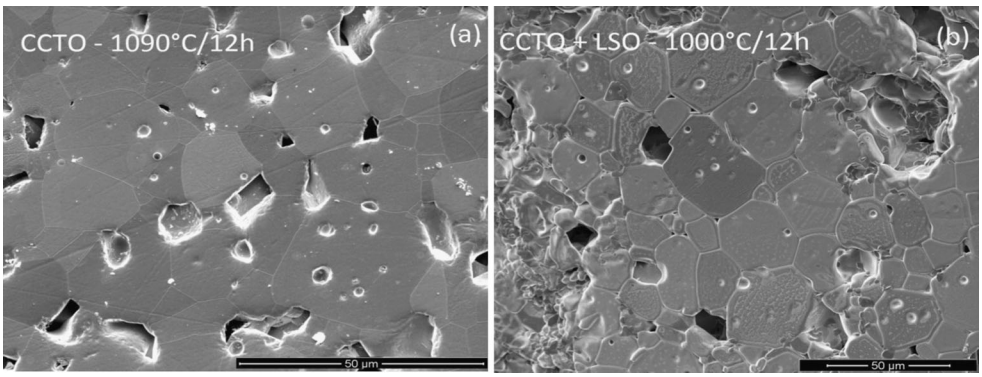

Fig. 7 FEG-SEM micrographs of CCTO **a** without LSO, sintered at 1090 °C and **b** with LSO sintered at 1000 °C

Table 2 Values of average grain size, G, dielectric permittivity, ε′, dielectric loss, tan δ, and capacitance of the grain boundaries, C of sintered CCTO specimens without and with LSO

Sintering profile (°C/h)	CCTO				CCTO + LSO			
	G (μm)	ε′	tan δ	C (nF cm^{-1})	G (μm)	ε′	tan δ	C (nF cm^{-1})
1000/12	–	–	–	–	24.4	13,910	0.225	1.23
1025/12	–	–	–	–	24.6	17,902	0.161	1.59
1050/12	–	–	–	–	25.3	20,122	0.153	1.78
1070/12	11.0	11,081	0.156	0.98	17.2	22,714	0.189	2.01
1080/12	16.6	5992	0.403	0.53	14.1	19,565	0.195	1.73
1090/12	23.4	11,792	0.391	1.04	22.0	93,767	0.524	8.30
1100/12	26.1	19,329	0.120	1.71	–	–	–	–

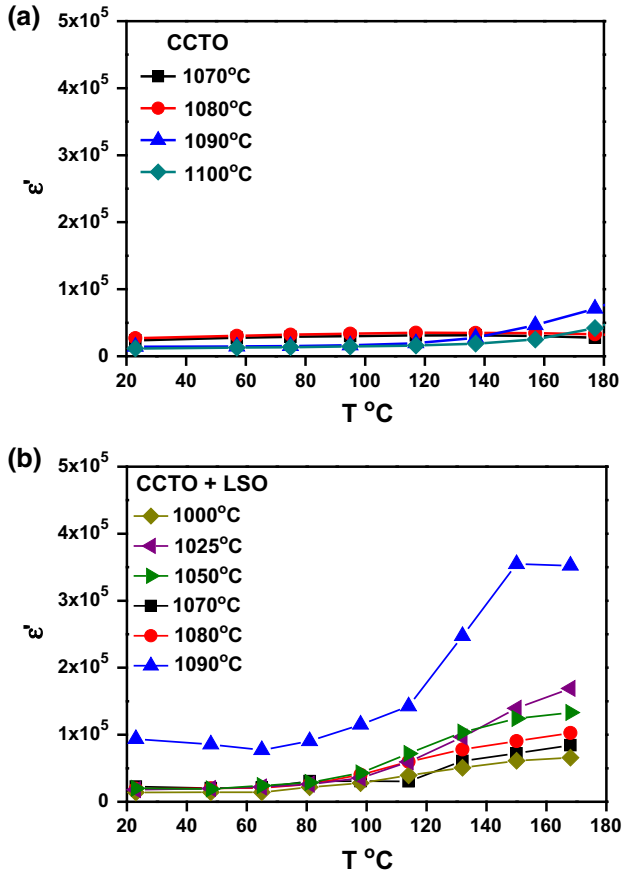

Fig. 8 Evolution of the electric permittivity with the temperature for specimens **a** without and **b** with LSO addition

specimens containing LSO, with dielectric loss of the same order of magnitude than those of specimens without additive. It is remarkably high the value of ε′ when the specimen containing the additive is sintered at 1090 °C, which is accompanied by an increase of the dielectric loss. In general, high vales of dielectric loss are attributed to heterogeneous conduction at the interfaces [13]. This effect reveals that at such high temperature significant changes occur at the grain boundaries, in agreement with the evaluated capacitance value.

The evolution of ε′ with the temperature is shown in Fig. 8 for specimens without (a) and with LSO (b).

Independent on the additive, the dielectric permittivity remains approximately constant up to 100 °C. The largest variation of ε′ with temperature is observed for CCTO containing LSO sintered at 1090 °C.

4 Conclusions

$CaCu_3Ti_4O_{12}$ mixed oxide was successfully synthesized by the coprecipitation method. After calcination at 800 °C for 4 h, the pure cubic perovskite phase was obtained. The overall results evidence the possibility to obtain this mixed oxide at low sintering temperatures with good densification and dielectric properties, by adding a small amount of lithium disilicate glass prior to sintering.

Acknowledgments The authors gratefully acknowledge FAPESP, CNPq and CNEN for financial support. One of the authors (T. C. Porfirio) acknowledges CNPq for the scholarship.

References

1. M.A. Subramanian, D. Li, N. Duan, B.A. Reisner, A.E. Sleight, J. Solid State Chem. **151**, 323 (2000)
2. J.R. Li, IEEE Trans. Dielectr. Electr. Insul. **11**, 534 (2004)
3. L.C. Kretly, A.F.L. Almeida, P.B.A. Fechini, R.S. De Oliveira, A.S.B. Sombra, J. Mater. Sci.: Mater. Electron. **15**, 657 (2004)
4. B.A. Bender, M.-J. Pan, Mater. Sci. Eng., B **117**, 339 (2005)
5. D.C. Sinclair, T.B. Adams, F.D. Morrison, A.R. West, Appl. Phys. Lett. **80**, 2153 (2002)
6. I. He, J.B. Neaton, M.H. Cohen, D. Vanderbilt, C.C. Homes, Phys. Rev. B **65**, 214112 (2002)
7. M.H. Cohen, J.B. Neaton, I. He, D. Vanderbilt, J. Appl. Phys. **94**, 3299 (2003)
8. A. Tselev, C.M. Brooks, S.M. Anlage, H. Zheng, L. Salamanca-Riba, R. Ramesh, M.A. Subramanian, Phys. Rev. B **70**, 144101 (2004)
9. R.K. Grubbs, E.L. Venturini, P.G. Clem, J.J. Richardson, B.A. Tuttle, G.A. Samara, Phys. Rev. B **72**, 104111 (2005)
10. S.V. Kalinin, J. Shin, G.M. Veith, A.P. Baddorf, M.V. Lovanov, H. Runge, M. Greenblatt, Appl. Phys. Lett. **86**, 102902 (2005)
11. T.-T. Fang, L.-T. Mei, H.-F. Ho, Acta Mater. **54**, 2867 (2006)
12. S. Kwon, C.-C. Huang, M.A. Subramanian, D.P. Cann, J. Alloy. Compd. **473**, 433 (2009)
13. M.A. de la Rubia, P. Leret, J. de Frutos, J.F. Fernández, J. Am. Ceram. Soc. **95**, 1866 (2012)
14. B.P. Zhu, Z.Y. Wang, Y. Zhang, Z.S. Yu, J. Shi, R. Xiong, Mater. Chem. Phys. **113**, 746 (2009)
15. B. Barbier, C. Combettes, S. Guillemet-Fritsch, T. Chartier, F. Rossignol, A. Rumeau, T. Lebey, E. Dutarde, J. Eur. Ceram. Soc. **29**, 731 (2009)
16. T.C. Porfirio, E.N.S. Muccillo, Adv. Mater. Res. **975**, 184 (2014)
17. R. Kashyap, O.P. Thakur, N.C. Mehra, R.P. Tandon, Int. J. Mod. Phys. B **25**, 1049 (2011)
18. Y. Hu, Y. Pu, P. Wang, J. Mater. Sci.: Mater. Electron. **25**, 546 (2014)
19. B. Shri Prakash, K.B.R. Varma, J. Solid State Chem. **180**, 1918 (2007)
20. B. Wang, Y. Pu, H. Wu, K. Chen, N. Xu, J. Mater. Sci.: Mater. Electron. **23**, 612 (2012)
21. S.K. Tadokoro, E.N.S. Muccillo, J. Alloy. Compd. **344**, 186 (2002)
22. J.L. Zhang, P. Zheng, C.L. Wang, M.L. Zhao, J.C. Li, J.F. Wang, Appl. Phys. Lett. **87**, 142801 (2005)
23. S.F. Shao, J.L. Zhang, P. Zheng, C.L. Wang, Solid State Comm. **142**, 281 (2007)
24. H. Fan, Q. Zheng, B. Peng, Mater. Res. Bull. **48**, 3278 (2013)
25. P. Thongbai, B. Putasaeng, T. Yamwong, V. Amornkitbamrung, S. Maernsiri, J. Alloy. Compd. **582**, 747 (2014)